Mechatronics 18 (2008) 495–505

Contents lists available at ScienceDirect

Mechatronics

journal homepage: www.elsevier.com/locate/mechatronics

Gain-scheduled robust control of a novel 3-DOF micro parallel positioning platform via a dual stage servo system

Tae Won Seo [a], Hwa Soo Kim [b], Deuk Soo Kang [a], Jongwon Kim [a,*]

[a] Seoul National University, School of Mechanical and Aerospace Engineering, Seoul 151-744, Republic of Korea
[b] University of Minnesota, Department of Mechanical Engineering, 111 Church Street, S.E. Minneapolis, MN 55455, USA

ARTICLE INFO

Article history:
Received 27 August 2007
Accepted 2 April 2008

Keywords:
Robust control
Gain scheduling
H_∞ control
Dual servo system
Micro positioning platform

ABSTRACT

This paper presents a gain-scheduled robust control of a micro positioning platform using a dual stage servo system, which recently has been developed to achieve the 3-DOF motions (x- and y-translations and α-tilting) with the accuracy to the sub-micrometer. The proposed platform consists of three sets of two-stage actuators: AC servo motors with ball screw for rough positioning and piezo actuators for fine positioning. Unlike existing parallel mechanisms using dual servo systems, the proposed platform is unique due to the fact that the actuation directions of the coarse and fine actuators are vertical with respect to each other, which enables them to effectively increase the mobility and resolution of the platform. While a well-known PI controller was adopted to establish the coarse control system due to its simplicity and reasonable performance, a gain-scheduled H_∞ controller was also employed to robustly ensure the desired accuracy of the fine control system. Since the coarse actuator is relatively slow and the mass of the proposed platform is negligible, the PI controller design for the coarse system is based on the kinematics of the proposed platform. Conversely, a physics-based dynamic model for the fine system is derived from a non-parametric system identification in order to match the experimental data well. Based on the combination of coarse and fine controllers, a dual servo control system is proposed, which sequentially selects the controller according to the pose of the proposed platform such as rotational angle, vertical and horizontal position. The successful performance of the synthesized controllers was verified through extensive experiments.

© 2008 Elsevier Ltd. All rights reserved.

1. Introduction

Since the demand has increased for commercial products that have greater functions in a smaller size, it is necessary to develop a micro factory capable of manufacturing and assembling micro-scale products. Most of the micro machining technologies are based mainly on semiconductor technology. However, semiconductor technology inevitably has limitations for manufacturing a complicated three-dimensional product because the semiconductor technology fundamentally stems from two-dimensional machining technologies. Therefore, traditional machining systems are employed to manufacture small three-dimensional shaped products, but in order to manufacture those small products, the size of the traditional machining system becomes considerably large, which leads to the loss of energy, space and time. In this respect, it is not surprising that many researchers have been putting significant effort into developing manufacturing systems for small products.

In recent decades, the parallel mechanisms have become attractive because they exhibit advantages in the manufacturing accuracy and speed. This plays an important role in developing the micro-scale positioning platform. Hasselbach et al. have investigated several positioning platforms based on a parallel mechanism and emphasized the advantages of a parallel mechanism in the precision positioning field [1]. Yi et al. have designed and conducted experiment on the stiffness of a platform consisting of several flexure hinges [2]. Takeda et al. have designed a parallel manipulator platform based on the Stewart–Gough platform using a dual stage actuation system [3].

However, the rotational capability of existing parallel mechanisms has been restricted so that the maximum rotational capability turns out to be less than 20 degrees. Such a low rotational capability is a representative disadvantage of parallel manipulators in comparison to serial ones. In order to improve the rotational capability of a parallel mechanism, several studies have been performed: Liu et al. have suggested a family of 3-DOF parallel mechanisms with high rotational capability of 100 degrees [4]. And Kim et al. have suggested a 6-DOF Eclipse-I and II mechanism that can rotate 90 and 360 degrees, respectively [5,6]. Kang et al. proposed the parallel mechanism

* Corresponding author. Fax: +82 2 875 4848.
E-mail address: jongkim@snu.ac.kr (J. Kim).

0957-4158/$ - see front matter © 2008 Elsevier Ltd. All rights reserved.
doi:10.1016/j.mechatronics.2008.04.002

presented in this paper, in which the rotational capability is up to 100 degrees [7].

To enhance manufacturing accuracy and speed, the controller design is a very important factor. For parallel mechanism platforms, many control algorithms are applied and verified for accuracy and speed. Choi et al. have applied a sliding mode controller to the 3-DOF parallel manipulator using electro-rheological value actuators and have experimentally verified the performance [8]. Callegari et al. have calculated dynamic modeling of a novel 3-RCC translational platform and have applied a hybrid position/force controller [9]. Li et al. have emphasized the difficulties in controlling parallel mechanisms and have insisted that by combining the design for control and a simple control algorithm, the mechanism can satisfy a performance [10]. Lee et al. have assumed that the nonlinear coefficient matrices of the Stewart platform are constant, and they designed a robust controller by supposing the assumption error is disturbance [11].

This paper presents a dual servo control of a novel 3-DOF (x- and y-translations and α-tilting) micro positioning platform. This platform guarantees compactness and simplicity in the structure as well as the motion accuracy to the sub-micrometer and an excellent tilting capability of more than 100 degrees in the performance. The dual servo system adopted in this paper consists of three AC servo motors employed to achieve a large workspace, specially with a high tilting angle. It also has three piezo actuators that are used to produce the positioning accuracy of the proposed micro positioning platform at the sub-micrometer scale.

For the coarse actuator control, a commercial PI controller was adopted due to its simplicity and reasonable performance. Since the coarse actuator is relatively slow compared to the fine actuator and the mass of the proposed micro platform is negligible, the PI controller design for the coarse system is carried out based on the kinematics of the proposed platform. It is noted that the position and the orientation of the micro positioning platform significantly influence the fine dynamics, while the coarse actuator is quite tolerable to those factors due to its relatively slow response. In order to guarantee the desired accuracy of a sub-micrometer in the presence of uncertainties such as those stemming from errors in manufacturing, assembling, and calibration, an H_∞ robust control technique was employed to design a fine controller for the stacked lead zirconate titanate (PZT) piezoelectric actuator. The first step to construct a fine control system is to establish a model that can predict the experimental data with high fidelity. To this end, the experimental transfer function for the fine dynamics was first obtained at the home position via a non-parametric system identification such as the empirical transfer function estimate (ETFE) [12]. Based on this home-position model, the uncertainties of the fine model under other positions were investigated and effectively described by the parametric variation. Then, a gain-scheduled H_∞ control was designed to ensure both robust stability and performance of the fine dynamics against the uncertainties [13–15]. The performance of the proposed sequential control scheme composed of PI controller for the coarse dynamics and the gain-scheduled H_∞ control for the fine dynamics is analyzed through the extensive experiments.

The proposed micro parallel positioning platform is described in Section 2. The mechanism is described and the problem is defined. And Section 3 presents kinematic and dynamic modeling for controller synthesis. The unknown parameters are estimated by experiment. In Section 4, the dual servo control is derived and simulation and experimental results are shown. Finally, conclusions are presented in Section 5.

2. Micro parallel positioning platform and problem definition

2.1. Mechanism description

The micro parallel mechanism platform can realize 3-DOF motion. It can translate along to the x- and y-axis and rotate to the α-axis (along the x-axis). The translational workspace is 5 mm × 5 mm and rotational workspace is 100 degrees. The parallel mechanism is proposed in Fig. 1. The mechanism is composed of an end-effector, three links and base platform. The base platform and end-effector are connected by two identical links and one parallelogram shaped link. The parallelogram shaped link can confine the rotation of the end-effector so the end-effector can only be rotated on the α-axis.

The actuation part consists of two sets of linear actuators: coarse and fine actuation. The coarse actuator shows a relatively long stroke and rough accuracy. The fine actuator shows a relatively short stroke and fine accuracy. The combination of these two kinds of actuation can result in a long stroke and fine accuracy. The coarse actuator is designed vertically to enhance the mobility of the mechanism and the fine actuator is designed horizontally to increase the resolution of the mechanism.

2.2. Manufacturing of the positioning platform

The micro positioning platform was manufactured and assembled in the lab., and the overview of the platform is shown in Fig. 2. The total size of the platform is 280(w) × 200(d) × 408(h) mm^3. For low friction movement, six unique universal joints are used. The universal joint is presented on the right side of Fig. 2.

To enhance and measure the accuracy of the platform, sensors are required. To measure the 3-DOF motion of the end-effector,

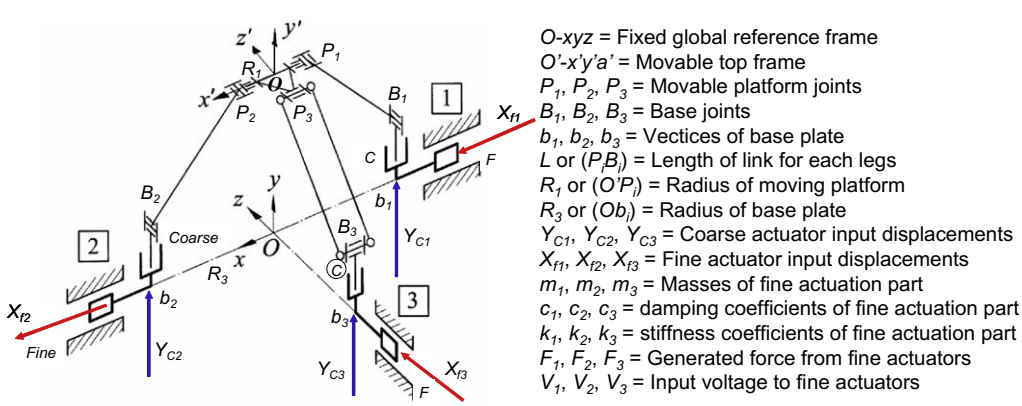

Fig. 1. 3-DOF parallel mechanism and actuation part.

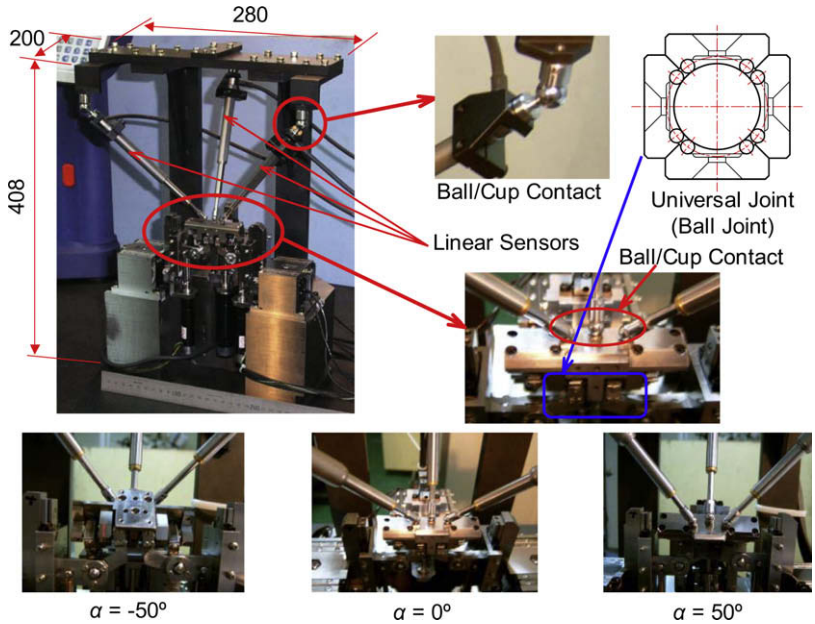

Fig. 2. Micro parallel positioning platform: sensors, universal joint and photos of rotation posture.

three linear scales are attached to the end-effector [16]. The sensors are shown in the left side of Fig. 2.

At the bottom of Fig. 2, the tilting capability of the positioning platform is presented. The photos show the tilting posture of the platform at −50, 0 and 50 degrees, respectively.

2.3. Problem definition

In this paper, the modeling and control for the micro parallel positioning platform are presented. For the coarse actuator control, the PI controller is adopted, and for the fine actuator control, the gain-scheduled H_∞ controller is designed. To combine the two kinds of controller, sequential control algorithm is used. The output of the end-effector is measured by three linear scales. The positioning accuracy of the platform has been verified through extensive experiments.

3. Modeling of micro parallel positioning platform

3.1. Constraint equation

The kinematic constraint of the mechanism is that the length of each link is constant as shown in Eq. (1).

$$\|\boldsymbol{P}_i - \boldsymbol{B}_i\| = L, \quad \text{where } i = 1,2,3 \tag{1}$$

Three scalar equations can be generated from Eq. (1) for the three links, respectively, as follows:

$$(x - R_1 + R_3 - X_{f1})^2 + (y - Y_{c1})^2 = L^2 \tag{2}$$

$$(x + R_1 - R_3 - X_{f2})^2 + (y - Y_{c2})^2 = L^2 \tag{3}$$

$$(-R_1\cos\alpha + R_3 - X_{f3})^2 + x^2 + (R_1\sin\alpha + y - Y_{c3})^2 = L^2 \tag{4}$$

By using these constraints, the forward and inverse kinematics can be calculated.

3.2. Jacobian matrix

A Jacobian matrix is necessary in order to derive the dynamic equation for the proposed micro platform. The Jacobian matrix is the relation of small perturbation of input and the response of output. By differentiate Eqs. (2)–(4), we have the equation in matrix form like follow:

$$\boldsymbol{J}_p\delta\boldsymbol{p} = \boldsymbol{J}_q\delta\boldsymbol{q} + \boldsymbol{J}_r\delta\boldsymbol{r} \tag{5}$$

where $\delta\boldsymbol{p}$, $\delta\boldsymbol{q}$ and $\delta\boldsymbol{r}$ represent $[\delta x \quad \delta y \quad \delta\alpha]^\top$, $[\delta X_{f1} \quad \delta X_{f2} \quad \delta X_{f3}]^\top$ and $[\delta Y_{c1} \quad \delta Y_{c2} \quad \delta Y_{c3}]^\top$ respectively. And $\boldsymbol{J}_p$, $\boldsymbol{J}_q$ and $\boldsymbol{J}_r$ represent the matrices like follow:

$$\boldsymbol{J}_p = \begin{bmatrix} x - R_1 + R_3 - X_{f1} & y - Y_{c1} & 0 \\ x + R_1 - R_3 + X_{f2} & y - Y_{c2} & 0 \\ x & y + R_1\sin\alpha - Y_{c3} & \boldsymbol{J}_p(3,3) \end{bmatrix}$$

$$\boldsymbol{J}_p(3,3) = (y + R_1\sin\alpha - Y_{c3})R_1\cos\alpha + (-R_1\cos\alpha + R_3 - X_{f3})R_1\sin\alpha$$

$$\boldsymbol{J}_q = \begin{bmatrix} x - R_1 + R_3 - X_{f1} & 0 & 0 \\ 0 & x + R_1 - R_3 + X_{f2} & 0 \\ 0 & 0 & -R_1\cos\alpha + R_3 - X_{f3} \end{bmatrix}$$

$$\boldsymbol{J}_r = \begin{bmatrix} y - Y_{c1} & 0 & 0 \\ 0 & y - Y_{c2} & 0 \\ 0 & 0 & R_1\sin\alpha + y - Y_{f3} \end{bmatrix}$$

Then the Jacobian matrix of the coarse and fine actuation is defined like follow:

$$\delta\boldsymbol{p} = \boldsymbol{J}_f\delta\boldsymbol{q} + \boldsymbol{J}_c\delta\boldsymbol{r}, \quad \text{where } \boldsymbol{J}_f = \boldsymbol{J}_p^{-1}\boldsymbol{J}_q \text{ and } \boldsymbol{J}_c = \boldsymbol{J}_p^{-1}\boldsymbol{J}_r \tag{6}$$

where the $\boldsymbol{J}_f$ denotes the Jacobian of fine actuators and $\boldsymbol{J}_c$ denotes Jacobian of coarse actuators.

3.3. Dynamic model of fine actuation system

3.3.1. Dynamic formulation

Note that the coarse actuator is relatively slow compared to the fine actuator and the mass of the proposed platform is negligible. Based on the kinematics of the proposed platform, the PI controller is then employed for the coarse system. However, since the position and the orientation of the micro positioning platform significantly influence the fine dynamics while the coarse dynamics is quite tolerable to those factors due to its relatively slow response, the dynamic model for the fine dynamics of the proposed micro platform is necessary to develop the fine controller.

Fig. 3 shows the schematic diagram for the fine dynamics of the proposed micro platform. Each PZT actuator is assumed to be the mass–spring–damper system. The masses of the links and the end-effectors are relatively negligible with respect to that of each PZT actuation part and are therefore considered as massless rigid bodies. The dynamic equation for each PZT actuation part is derived as follows:

$$F_i - k_i X_{fi} - c_i \dot{X}_{fi} = m_i \ddot{X}_{fi}, \quad \text{where } i = 1, 2, 3 \tag{7}$$

By combining these independent dynamic equations and the Jacobian matrix in Eq. (6), the state-space dynamic model for the fine system of the micro parallel positioning platform is obtained as follows:

$$\begin{aligned} \dot{\boldsymbol{x}} &= \boldsymbol{A}\boldsymbol{x} + \boldsymbol{B}\boldsymbol{u}, & \boldsymbol{x} &= [X_{f1}\ \dot{X}_{f1}\ X_{f2}\ \dot{X}_{f2}\ X_{f3}\ \dot{X}_{f3}]^\top \\ \boldsymbol{y} &= \boldsymbol{C}\boldsymbol{x}, & \boldsymbol{u} &= [F_1\ F_2\ F_3]^\top, \quad \boldsymbol{y} = [x\ y\ \alpha]^\top \end{aligned} \tag{8}$$

where

$$\boldsymbol{A} = \begin{bmatrix} 0 & 1 & 0 & 0 & 0 & 0 \\ -\frac{k_1}{m_1} & -\frac{c_1}{m_1} & 0 & 0 & 0 & 0 \\ 0 & 0 & 0 & 1 & 0 & 0 \\ 0 & 0 & -\frac{k_2}{m_2} & -\frac{c_2}{m_2} & 0 & 0 \\ 0 & 0 & 0 & 0 & 0 & 1 \\ 0 & 0 & 0 & 0 & -\frac{k_3}{m_3} & -\frac{c_3}{m_3} \end{bmatrix}, \quad \boldsymbol{B} = \begin{bmatrix} 0 & 0 & 0 \\ \frac{1}{m_1} & 0 & 0 \\ 0 & 0 & 0 \\ 0 & \frac{1}{m_2} & 0 \\ 0 & 0 & 0 \\ 0 & 0 & \frac{1}{m_3} \end{bmatrix}$$

$$\boldsymbol{C} = \begin{bmatrix} \boldsymbol{J}_f(1,1) & 0 & \boldsymbol{J}_f(1,2) & 0 & \boldsymbol{J}_f(1,3) & 0 \\ \boldsymbol{J}_f(2,1) & 0 & \boldsymbol{J}_f(2,2) & 0 & \boldsymbol{J}_f(2,3) & 0 \\ \boldsymbol{J}_f(3,1) & 0 & \boldsymbol{J}_f(3,2) & 0 & \boldsymbol{J}_f(3,3) & 0 \end{bmatrix}$$

The relation between the voltage input V_i to the PZT actuator and the force F_i generated by the PZT actuator is examined by experiments and may be described as follows. Fig. 4 shows the experimental relation between the voltage input to the PZT and the force generated by the PZT.

$$V_i = \frac{F_i}{1000}, \quad \text{where } i = 1, 2, 3 \tag{9}$$

3.3.2. Parameter estimation

The authors set up the dynamic formulation of the micro parallel positioning platform. However, in order to synthesize the

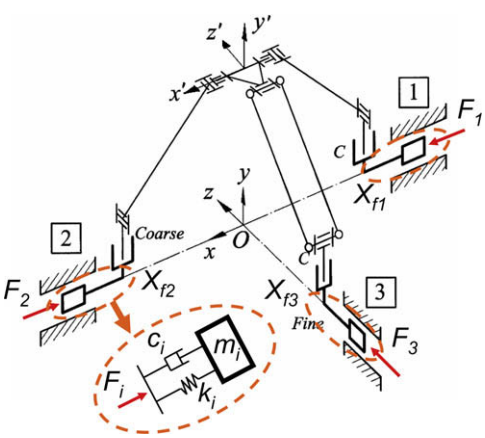

Fig. 3. Relation of force and dynamic response.

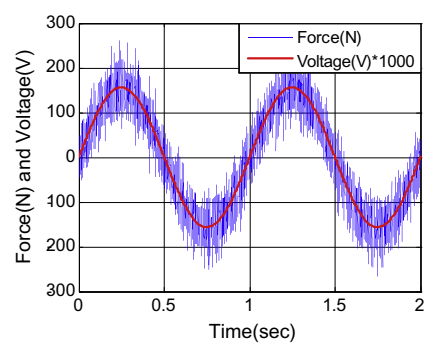

Fig. 4. Relation between input voltage and generated force.

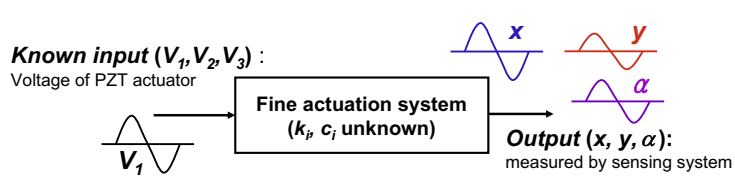

Fig. 5. Experimental process of parameter estimation.

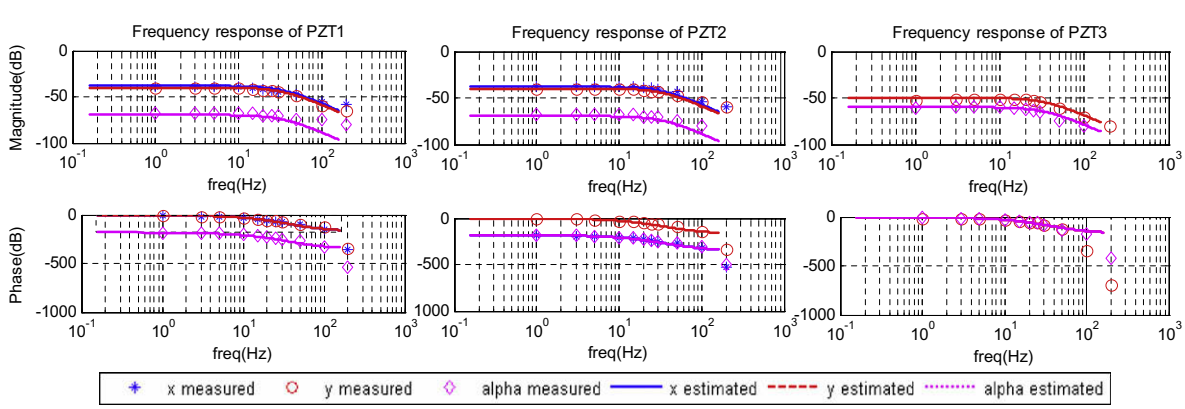

Fig. 6. Parameter estimation result and frequency response of estimated transfer function.

Table 1
Estimated coefficient

Coefficient	m_i (kg)	c_i (N/μm s)	k_i (N/μm)
Value	0.804	0.00816	1.00

controller, the stiffness and damping coefficients of the dynamic model are firstly identified so that the resulting model for the proposed micro platform predicts the experimental data with high fidelity.

Since the dynamic formulation depends on the pose transfer (x, y and α pose), we have conducted the experiment at the home position to obtain the model to be used for synthesizing the controller. The process is shown in Fig. 5. To ignore the nonlinear properties like backlash, we used sinusoidal inputs of several frequencies, not white noise. Then we measured the magnitude change and phase delay of each sinusoidal input. The transfer relation at the home position was then obtained. These are represented as star, circle and diamond shaped points in Fig. 6.

Next, the damping and stiffness coefficients are adjusted and the bode plot of the transfer function is checked to match the state-space model and experimental result. To simplify the dynamic model, the mass, damping and stiffness coefficients are the same value in each link, respectively. The estimated mass, damping and stiffness coefficients are presented in Table 1.

The transfer function of the micro parallel positioning platform at the home position is shown in Eq. (10). The frequency response of the model is represented by the solid lines in Fig. 6.

The transfer function matrix at the home position is composed of nine transfer functions. The transfer function from V_3 to x is assumed to be zero since the relative magnitude of the transfer function is much lower than other transfer functions.

$$\begin{bmatrix} x \\ y \\ \alpha \end{bmatrix} = \begin{bmatrix} \frac{621.9}{s^2+406.1s+49750} & \frac{-621.9}{s^2+406.1s+49750} & 0 \\ \frac{510.4}{s^2+406.1s+49750} & \frac{510.4}{s^2+406.1s+49750} & \frac{161.7}{s^2+406.1s+49750} \\ \frac{-16.52}{s^2+406.1s+49750} & \frac{-16.52}{s^2+406.1s+49750} & \frac{50.05}{s^2+406.1s+49750} \end{bmatrix} \begin{bmatrix} V_1 \\ V_2 \\ V_3 \end{bmatrix} \tag{10}$$

4. Control of the micro parallel positioning platform

4.1. Coarse actuator control

For the coarse actuation, we selected the MAS-D16H20 and MAS-D23H25 as the coarse actuators and BSD-11 as the coarse actuator controller (Chiba Precision Co.). The actuator consists of AC servo motors with ball screws and a PI controller for each actuator is designed based on the kinematics. The position reference is commanded by the pulse signal. The detailed specifications of the coarse actuator are summarized in Table 2.

Since a PI controller is used for each positioning control of three coarse actuators, a total of six controller gains have to be tuned. Taguchi methodology was used for control gain tuning.

4.2. Fine actuator control

4.2.1. Problem of dynamics change and strategy of controller synthesis

In Section 3.3, the dynamic model for the fine system of the proposed micro platform was derived. The corresponding physical parameters were identified so that the resulting transfer function predicts the experimental data with a high fidelity. However, it turns out that the dynamics of the proposed micro platform significantly change according to the position of its end-effector in the workspace and in particular, α-directional tilting considerably affects the dynamics. According to the assumption in Section 3.3, the dynamic characteristics including the stiffness and damping coefficients of the micro platform do not change considerably along the position of the end-effector. On the contrary, the kinematic characteristics such as the Jacobian matrix highly depend on the position of the end-effector so that the magnitude of the corresponding transfer function at each position changes without the variations of the corresponding phase. Fig. 7 shows the variations of the transfer function from PZT ♯3 to y-directional movement according to the α-directional pose transfer. It turns out that the corresponding phase does not change according to the pose transfer except for the case when α is -45 degrees.

Some geometric error factors of the micro parallel positioning platform may occur and stem from manufacturing, assembling and calibration errors but it is difficult to explicitly account for such kinematic variations of the micro platform only by using the kinematic relationship. Therefore, we have conducted several experiments under the condition of pose change according to the procedure explained in Section 3.3. In every case, the phase obtained from the experiment exactly matches one from the prediction except for the transfer function from PZT ♯3 to y-directional movement. The variations of the magnitude along the x-directional pose change and α-directional pose change are shown in the left and right side of Fig. 8, respectively. The variation of the magnitude caused by y-directional pose change is negligible compared to those by x-directional pose change and α-directional pose change.

The deviations of the magnitude variation are shown in the upper right side of each figure. While the magnitude of x-directional movement significantly changes under x-directional pose change, both the magnitude of y- and α-directional movement

Table 2
Specifications of the coarse actuators

Photo		MAS-D16H20	MAS-D23H25
	Size (mm)	∅16 × 82	∅23 × 114
	Stroke (mm)	20	25
	Thrust (kg)	2	3
	Resolution (μm)	0.25	0.016
	Max. speed (mm/s)	4	5
	Screw lead (mm)	0.4	0.5
	Unidirectional repeatability (μm)	3	3
	Bidirectional repeatability (μm)	8	8
	Average reversal error (μm)	5	5
	Limit sensor	Hall sensor	Hall sensor
	Actuator No.	♯1 and ♯2	♯3

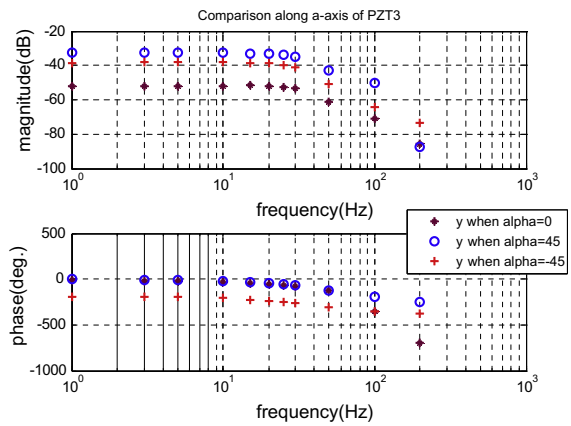

Fig. 7. Dynamic models from PZT ♯3 to y-directional movement along toward the α-directional pose transfer.

change under α-directional pose change. The largest deviations are written in bold red characters.

In order to not only achieve the accuracy of the sub-micrometer but also overcome the varying dynamics according to the position of the end-effector, a gain-scheduled H_∞ controller for the fine system of the proposed micro platform was adopted. The control block diagram is shown in Fig. 9. The controller design procedure is shown in Fig. 10. The H_∞ controller was designed at the home position to achieve such design specifications as accuracy and time response. Similarly, the H_∞ controllers for other models were synthesized in the other positions obtained in Section 3.3 based on the same design specifications. Then the designed robust controllers were smoothly connected to each other with an appropriate gain function. Based on the analysis of deviation of magnitude change, the x-directional controller gain was scheduled along to the x-pose change, and y- and α-directional controller gains were scheduled along toward the α-pose change.

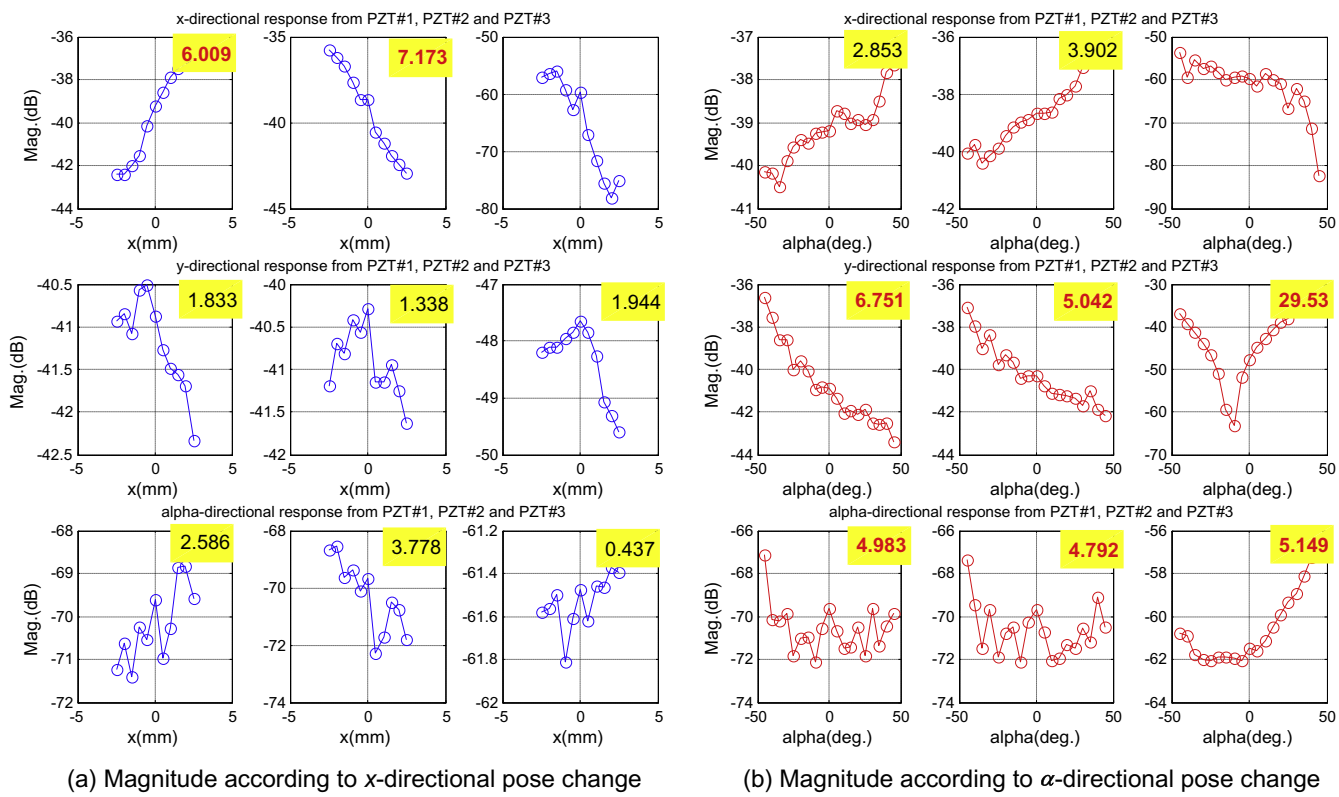

(a) Magnitude according to x-directional pose change (b) Magnitude according to α-directional pose change

Fig. 8. Magnitude change according to the x- and α-directional pose change.

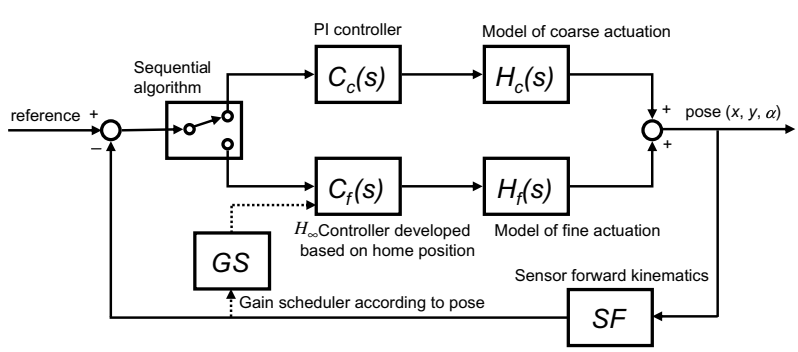

Fig. 9. Controller block diagram.

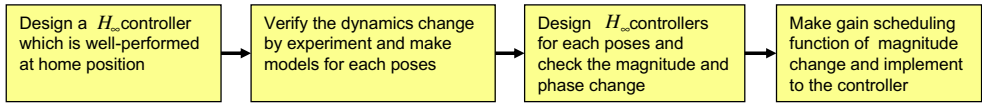

Fig. 10. Procedure of controller synthesis.

4.2.2. H_∞ controller based on home position

The synthesis of the fine controller was based on the dynamic model for the fine dynamics of the proposed micro platform at the home position in Eq. (10). The H_∞ controller was chosen to guarantee the desired accuracy of the sub-micrometer in the presence of uncertainties such as manufacturing or assembling error and calibration error. The sensitivity and complementary sensitivity transfer matrices are denoted $\boldsymbol{S}$ and $\boldsymbol{T}$, respectively. $\boldsymbol{S}$ and $\boldsymbol{T}$ are defined as follows:

$$\begin{aligned}\boldsymbol{S}(s) &= [\boldsymbol{I} + \boldsymbol{C}(s)\boldsymbol{H}(s)]^{-1}\\ \boldsymbol{T}(s) &= \boldsymbol{C}(s)\boldsymbol{H}(s)[\boldsymbol{I} + \boldsymbol{C}(s)\boldsymbol{H}(s)]^{-1}\end{aligned} \tag{11}$$

where $\boldsymbol{C} \in R^{3\times3}$ is the matrix of the fine controller to be designed and $\boldsymbol{H} \in R^{3\times3}$ is the matrix of the fine dynamic model for the proposed micro platform at the home position, respectively. From the control design point of view, the sensitivity transfer function from the tracking error to the displacement (along to the x- or y-axis) or the rotational angle output (along α-axis) must be small but the complementary transfer function from the voltage input to PZT to same output must be large. In order to mathematically describe these performance and robustness specifications, the following frequency weighting functions are typically adopted in the frame of H_∞ control design. The frequency weighting functions are defined as follows:

$$\boldsymbol{W}_p = \begin{bmatrix} \frac{0.667s+157}{s+0.01} & 0 & 0 \\ 0 & \frac{0.667s+157}{s+0.01} & 0 \\ 0 & 0 & \frac{0.4s+157}{s+0.01} \end{bmatrix},$$
$$\boldsymbol{W}_t = \begin{bmatrix} \frac{s+285}{0.316s+219} & 0 & 0 \\ 0 & \frac{s+285}{0.316s+219} & 0 \\ 0 & 0 & \frac{s+285}{0.316s+219} \end{bmatrix} \tag{12}$$

As pointed out previously, the frequency weighting functions $\boldsymbol{W}_p$ and $\boldsymbol{W}_t$ denote weighting on disturbance rejection and reference tracking, respectively. The magnitude plot of each weighting is shown in Fig. 11. $\boldsymbol{W}_p$ is constructed to attenuate the disturbances in the low frequency region maximally up to −40 dB at 1 Hz and $\boldsymbol{W}_t$ is designed to guarantee the frequency band of 35 Hz. Then, the robust controller design problem is to choose a controller $\boldsymbol{C}$ such that the closed-loop transfer function, i.e., the complementary transfer function is robustly stable and the following condition (robust performance index) holds:

$$|\boldsymbol{W}_p\boldsymbol{S}|_\infty + |\boldsymbol{W}_t\boldsymbol{T}|_\infty < 1 \tag{13}$$

Via the H_∞ synthesis algorithm, nine controllers are designed for the home-position model. Through the model truncation technique, nine third order H_∞ controllers are obtained without the performance degradation. The bode plot of the synthesized controller is shown in Fig. 12. And the step response is simulated and measured. For the fine actuators, we used PX38SG (Piezojena Co.), whose specifications are shown in Table 3. The step response of the controller

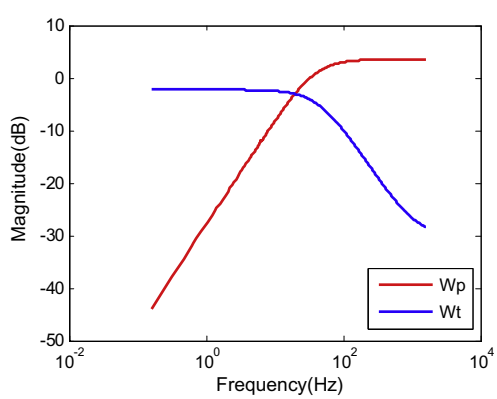

Fig. 11. Magnitude plot of weightings.

Table 3
Specifications of the fine actuator

Photo		
	Dimension (L × W × H) (mm)	40 × 40 × 25
	Stroke (μm)	32 (closed loop)
	Max. load (N)	100
	Force generation (N)	30
	Resolution (nm)	0.05
	Operating voltage (V)	−10 to 150
	Repeatability (nm)	23
	Nonlinearity (%)	0.1
	Stiffness (N/μm)	1
	Resonant frequency (Hz)	760
	Rotational error (μrad)	10
	Weight (g)	77

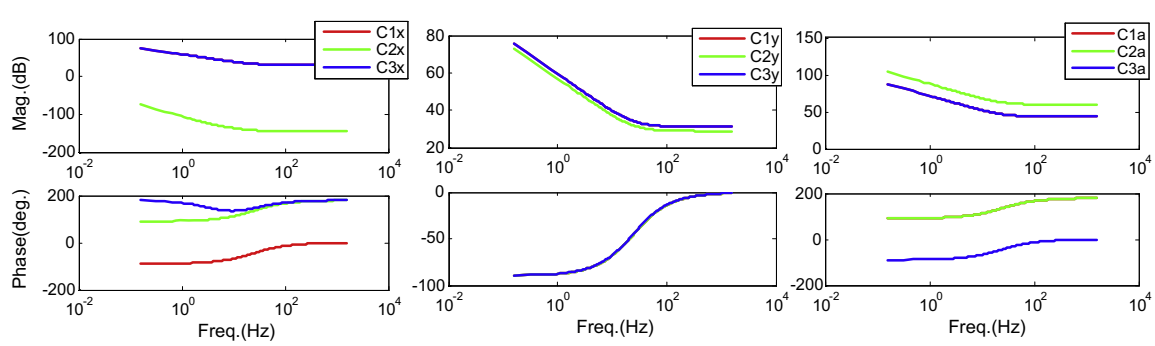

Fig. 12. Synthesized H_∞ controller based on home-position model.

from the simulation and experiment is each shown in Fig. 13. From the experimental results, the controller shows 2.66%, 4.69% and 6.12% of overshoot and 0.016 s, 0.022 s and 0.010 s of settling time in x-, y- and α-directional movement, respectively.

4.2.3. Gain-scheduled H_∞ controller

In the home position, satisfactory controller performance was achieved by using the H_∞ controller. However, as mentioned in Section 4.2.1, the fine dynamics varies according to the pose change, which leads to designing the gain-scheduled robust controller without sacrificing the performance.

The fine system models for the proposed micro platform at each pose are shown in Fig. 8. Based on these models, a novel gain scheduling functions are constructed as shown in Fig. 14. While the upper two gains which influence the x-directional movement are the functions of x-pose change and the other six gains which influence y- and α-directional movement are the functions of α-pose change. The gain scheduling function from PZT ♯1 and PZT ♯2 to α-directional movement has switching surface at the α pose equals to -15 degrees.

The performance of the gain scheduling is experimentally verified. To generate the poses that can guarantee the robustness of the controller, the verification experiment poses are selected by using an $L_9(3^4)$ orthogonal array. The objective value is selected as the smaller-the-better S/N (signal to noise) ratio as follow:

$$S/N = -10\log\left|\frac{\sum y_i^2}{n}\right| \tag{14}$$

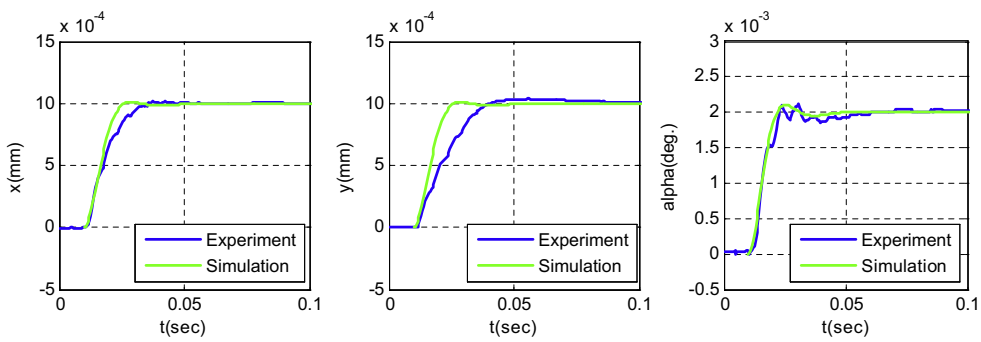

Fig. 13. Step response of the H_∞ controller at the home position.

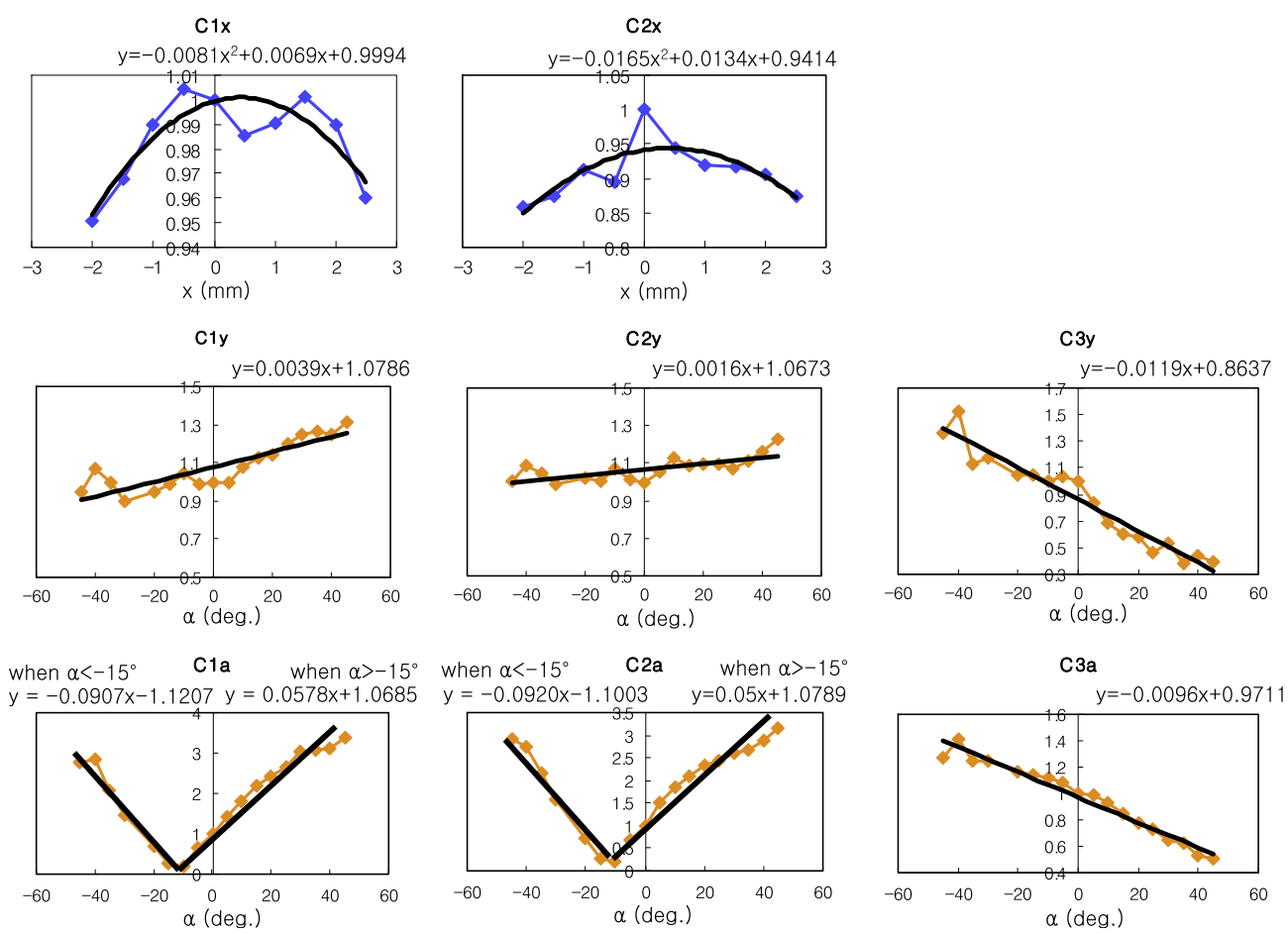

Fig. 14. Gain scheduling functions.

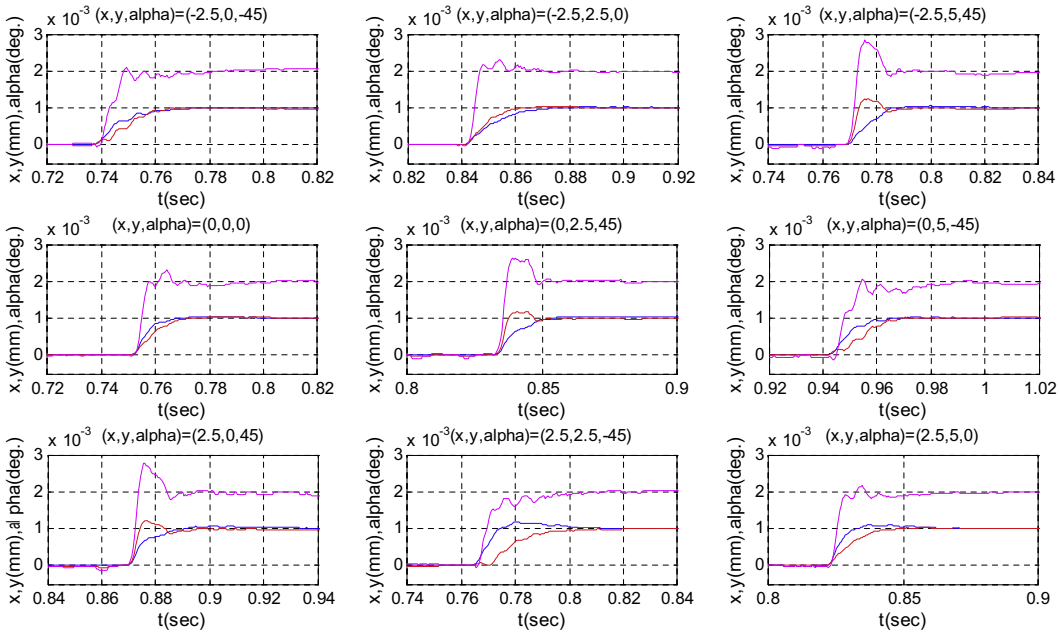

(a) Step response in various poses without gain scheduling

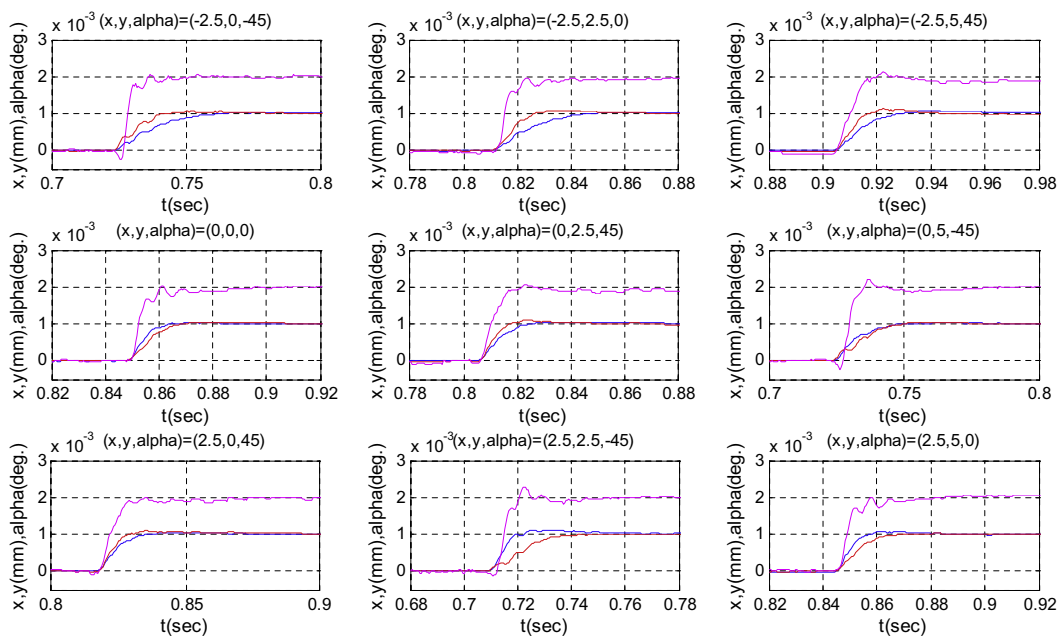

(b) Step response in various poses with gain scheduling

Fig. 15. Step response of fine actuation system.

The experimental result is presented in Fig. 15. Fig. 15a shows the step response without the gain scheduling and Fig. 15b shows the step response with gain scheduling in various poses which are generated based on $L_9(3^4)$ orthogonal array. The experimental result of overshoot and settling time is shown in Fig. 16[1] where the blue line with triangles shows the result without gain scheduling and the red line with circles shows the result with gain scheduling. In the case of overshoot, there is improvement of 5.33 dB. In the case of settling time, there is improvement of 1.31 dB.

[1] For interpretation of color in Figs. 1–8, 10–16 and 18, the reader is referred to the web version of this article.

4.3. Integrated dual servo control algorithm

4.3.1. Sequential control algorithm

The machine has three sets of two-stage linear actuators: a linear motor for rough positioning and a piezo actuator for fine positioning. What makes it unique is that the actuation directions of the coarse and fine actuators are vertical with each other to maximize the platform mobility and resolution. To use the mechanism as a positioning platform, we have to integrate the developed PI controller and H_∞ controller. However, the direction of the coarse and the fine actuators are perpendicular each other, so it is relatively hard to design a dual servo controller which considers the dynamic characteristics. Therefore, we adopt the switching type of controller to integrate the coarse and fine controllers.

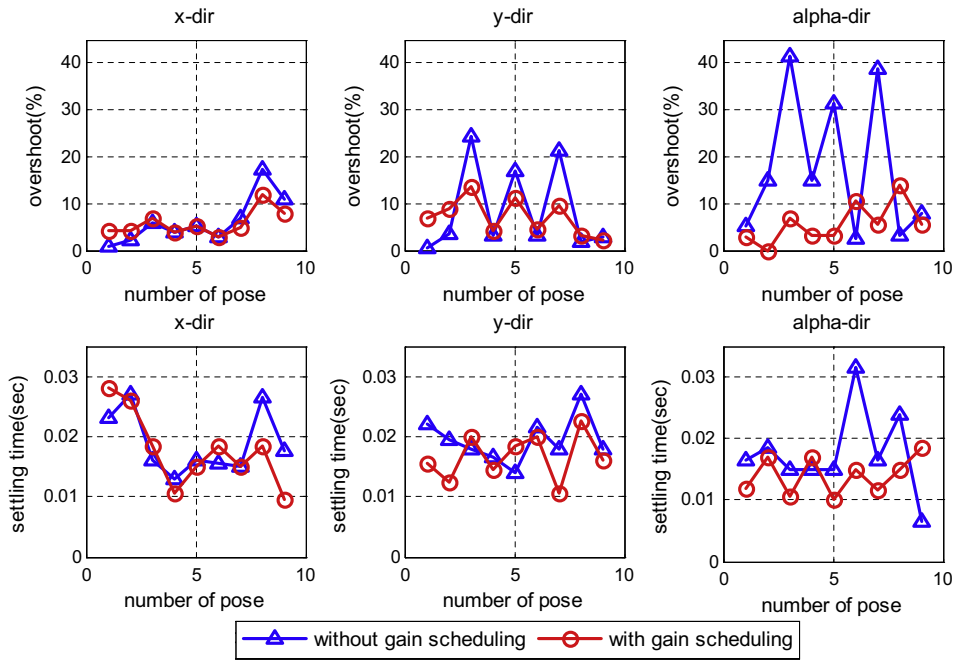

Fig. 16. Overshoot and settling time in each poses.

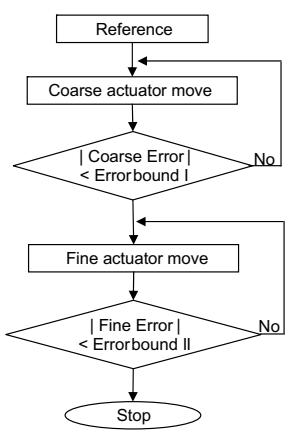

Fig. 17. Switching algorithm of dual stage system.

Fig. 17 shows the control algorithm of the sequential controller that is operated by the switching function. The switching algorithm has the advantage that at every control sampling period, the dual servo control algorithm block selects three coarse actuators first and executes the positioning control of the three coarse actuators simultaneously. If the positioning accuracy is within 5 μm (x- and y-axis) and 0.01 degree (α-axis), then the dual servo control algorithm selects three fine actuators in sequence and executes the positioning control of the three fine actuators simultaneously. If the positioning accuracy is within 0.1 μm (x- and y-axis) and 0.002 degree (α-axis), then the controller waits for the next reference signals. The sampling period is 100 ms.

4.3.2. Experimental result on positioning control

By using the switching control algorithm as the dual servo control algorithm, the experiment on positioning along to the circular path is conducted. Fig. 18 presents the experimental result for verifying the positioning control capabilities of the developed micro positioning platform. Graphs (a), (b) and (c) in Fig. 18 show the contouring accuracy of the platform in the x–y plane at three typical tilting angles of $\alpha = 0$, 45 and −45 degrees, respectively. The overall accuracy is within 0.3 μm. Graphs (d), (e) and (f) in Fig. 18 show the tilting capacity of the platform in the α-axis. The tilting angle range of ±45 degrees in the α-axis is achieved with the contouring accuracy within 0.9 μm on the basis of the extreme outer edge of the rotating platform, whose relative accuracy in μm unit was compatible with the contouring accuracy in the x- and y-axis. The feed rate in the x- and y-axis is 6 mm/min and that in the α-axis is 48 degrees/min.

5. Conclusions

This paper presented the dynamic modeling and controller synthesis for a 3-DOF micro parallel positioning platform. With regards to the geometric constraints of the structure, a Jacobian matrix was calculated as the dynamic relation and a simple spring–damper model was calculated from the fine actuator assumption. Based on the two results, state-space model for fine actuator was formulated. To estimate the damping and stiffness coefficients, the experiment was performed using a sinusoidal input. For the coarse actuator control, a PI controller was used, and for the fine actuator control, an H_∞ controller was designed. To overcome the dynamics change along with the pose transfer, a gain scheduling technique was integrated with the H_∞ controller for fine actuator control. For the dual servo control, sequential control algorithm was implemented and a positioning experiment was performed. Our analysis showed 0.294 μm of translational positioning accuracy and 0.827 μm of translational and rotational positioning accuracy. In the near future the dual servo controller for reference tracking is planning to be developed for application on micro laser machining.

Acknowledgement

This work is sponsored by the Brain Korea 21 program and Engineering Research Center for Micro-thermal Systems.

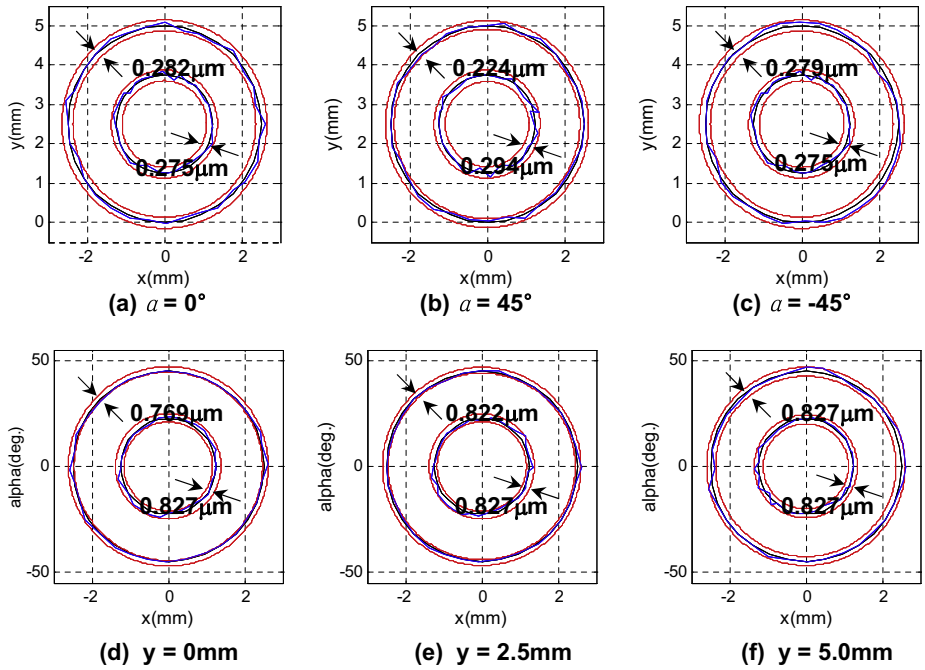

Fig. 18. Experimental result of the positioning along the circular path.

References

[1] Hasselbach J, Wreqe J, Raatz A, Becker O. Aspects on design of high precision parallel robots. Automation 2004;24(1):49–57.

[2] Yi BJ, Na HY, Chung GB, Kim WK, Suh IH. Design and experiment of 3 DOF parallel micro-mechanism utilizing flexure hinges. In: Proceedings—IEEE international conference on robotics and automation, vol. 2, 2002. p. 1167–72.

[3] Takeda Y, Funabashi H, Ichikawa K, Hirose K. An in-parallel actuated manipulator with redundant actuators for gross and fine motions. In: Proceedings—IEEE international conference on robotics and automation, vol. 1, 2003. p. 749–54.

[4] Liu X-J, Wang J, Pitschow G. A new family of spatial 3-DoF fully-parallel manipulators with high rotational capability. Mech Machine Theory 2005;40(4):475–94.

[5] Kim J, Park FC, Ryu SJ, Kim JW, Hwang JC, Park CB, et al. Design and analysis of a redundantly actuated parallel mechanism for rapid machining. IEEE Trans Robot Automat 2001;17(4):423–34.

[6] Kim J, Hwang JC, Kim JS, Iurascu C, Park FC, Cho YM. Eclipe-II: a new parallel mechanism enabling continuous 360-degree spinning plus three-axis translational motions. IEEE Trans Robot Automat 2002;18(3): 367–73.

[7] Kang DS, Seo TW, Yoon YH, Shin BS, Liu X-J, Kim J. A micro-positioning parallel mechanism platform with 100-degree tilting capability. Annals CIRP 2006;55(1):377–80.

[8] Choi SB, Park DW, Cho MS. Control of a parallel link manipulator using electro-rheological valve actuators. Mechatronics 2001;11(2):147–81.

[9] Callegari M, Palpacelli M-C, Principi M. Dynamic modeling and control of the 3-RCC translational platform. Mechatronics 2006;16(10):589–605.

[10] Li Q, Wu FX. Control performance improvement of a parallel robot via the design for control approach. Mechatronics 2004;14(8):947–64.

[11] Lee SH, Song JB, Choi WC, Hong D. Position control of a Stewart platform using inverse dynamics control with approximated dynamics. Mechatronics 2003;13(6):605–19.

[12] Ljung J. System identification theory for the user. Englewood Cliffs (NJ): Prentice-Hall; 1999.

[13] Skogestad S, Postlethwaite I. Multivariable feedback control. New York: Wiley; 1996.

[14] Doyle JC, Francis BA, Tannenbaum AR. Feedback control theory. Macmillan Publishing Company; 1992.

[15] Zhou K, Doyle JC. Essentials of robust control. Englewood Cliffs (NJ): Prentice-Hall; 1998.

[16] Kang DS, Seo TW, Yoon YH, Kim J. A micro-positioning platform with high tilting capability and its kinematic calibration. In: Proceeding of international conference on positioning technology, 2006.